Volume 1 | Number 1 | Jan 2013 | Pages 1–100

Journal of
Materials Chemistry A

Materials for energy and sustainability
www.rsc.org/materialsA

Li⁺

ROYAL SOCIETY
OF CHEMISTRY

ROYAL SOCIETY
OF CHEMISTRY

www.rsc.org/materialsA

Journal of Materials Chemistry A

ARTICLE

Improved dehydrogenation properties of the LiNH₂−LiH system by doping alkali metal hydroxide

Bao-Xia Dong, Jun Ge, Yun-Lei Teng*, Jing-Jing Gao, Liang Song

In this study, the hydrogen desorption properties of the LiNH₂−LiH system with alkali metal hydroxide (LiOH, NaOH, and KOH) were investigated and discussed. It was found that the three kinds of hydroxides are effective to enhance the hydrogen desorption properties of the LiNH₂−LiH system, among which, KOH shows the best effect. In comparison with the broad shaped hydrogen desorption curve of the LiNH₂−LiH system without additive, the hydrogen desorption curve of the LiNH₂−LiH−0.05 KOH composite becomes narrow. By doping 5 mol% KOH, the dehydrogenation onset temperature of the LiNH₂−LiH composite is decreased by about 36 °C, and the dehydrogenation peak temperature is lowered by about 42 °C. Detailed structural investigations reveal that during ball milling, the doped alkali metal hydroxide can react with LiH to convert to alkali metal hydride, which is responsible for the improvement in hydrogen desorption properties of LiNH₂−LiH system.

Introduction

Hydrogen, the most frequently discussed source, which only produces water after burnt in air, is now considered to be the most promising fuel in the future. The interest in hydrogen as energy of the future is due to it being a clean form of energy, and the most abundant element in the universe, the lightest fuel, richest in energy per unit mass.[1] However, there are still many problems to be solved if we want to make the hydrogen economy into reality because of the bottleneck about hydrogen storage. Conventional high pressure storage and cryo-storage are not suitable ways for practical vehicular application due to their hazardous properties and their low volumetric energy density. For example, compressed hydrogen at 70 MPa (300 K) is 4.7 kJ/cm³ and liquid hydrogen at 20 K (0.1 MPa) is 8.5 kJ/cm³, much lower than that of gasoline (34.9 kJ/cm³) or liquid natural gas (25.1 kJ/cm³).[2,3] As compared to approaches such as compression and liquefaction, solid-state hydrogen storage, especially for light element containing systems, is able to realize the high gravimetric and volumetric hydrogen densities.[4,5]

Metal–N–H hydrogen storage system has been investigated over the world since it was first reported by Chen *et al* in 2002, who indicates that Li₃N reversibly stores over 10 mass% hydrogen in the two consecutive reactions (reaction 1).[6]

$$Li_3N + 2H_2 \leftrightarrow Li_2NH + LiH + H_2 \leftrightarrow LiNH_2 + 2LiH \quad (1).$$
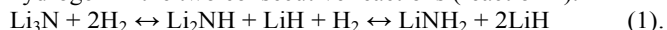
Later, the lithium amide (LiNH₂)−lithium hydride (LiH) system was also proposed as a sound solid-state storage system, as it can more easily absorb/desorb 6.5 mass% of hydrogen (reaction 2).[7,8] Whilst this system exhibits a relatively advantageous

$$Li_2NH + H_2 \leftrightarrow LiNH_2 + LiH \quad (2).$$
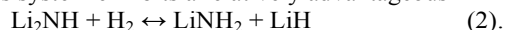
set of target thermodynamic parameters, the temperatures required for the dehydrogenation of lithium amide and the hydrogenation of lithium imide are still too high for the application of this system as a commercial hydrogen store.

Various efforts have been devoted to improving its hydrogen absorption and desorption kinetics.[9–19] Additives, such as titanium compounds, metal borohydrides, metal oxides and carbon-based materials were found to be effective in improving the hydrogen storage properties of the LiNH₂−LiH system. It was demonstrated recently that potassium compounds, including potassium hydride, potassium amide, potassium hydroxide and potassium halides, possess superior catalytic effects on the improvement of hydrogenation/dehydrogenation kinetics of Li–Mg–N–H system.[20–24] Moreover, it was also reported that the hydrogen desorption/absorption kinetics for the LiH–NH₃ system can be improved drastically by the addition of 5 mol% KH or KNH₂.[25] It is interesting to examine the catalytic effect of potassium compounds on the LiNH₂−LiH system.

In the present work, the hydrogen desorption properties of the LiNH₂−LiH system with alkali metal hydroxide (LiOH, NaOH, and KOH) were investigated and discussed. It was found that the three kinds of hydroxides are effective to enhance the hydrogen desorption properties of the LiNH₂−LiH system, among which, KOH shows the best effect. In comparison with the broad shaped hydrogen desorption curve of the LiNH₂−LiH system without additive, the hydrogen desorption curve of the LiNH₂−LiH−0.05 KOH composite becomes narrow. By doping 5 mol% KOH, the dehydrogenation onset temperature of the LiNH₂−LiH composite is decreased by about 36 °C, and the dehydrogenation peak temperature is lowered by about 42 °C. Detailed structural investigations reveal that during ball milling, the doped alkali metal hydroxide can react with LiH to convert to alkali metal hydride, which is responsible for the improvement in hydrogen desorption properties of LiNH₂−LiH system.

Experimental

2.1 Sample preparation

Lithium hydride (LiH) (98%, J&K Chemical Ltd., China), lithium amide (LiNH$_2$) (95%, Aldrich) were used for the following experiments. As additives, lithium hydroxide (LiOH) (99.5%, Sinopharm, China), sodium hydroxide (NaOH) (99.5%, Sinopharm, China), potassium hydroxide (KOH) (99.5%, Sinopharm, China), potassium hydride (KH) (Alfa Aesar, China) and lithium oxide (Li$_2$O) (98%, J&K Chemical Ltd., China) were chosen. The additives were dispersed into the samples by the following mechanical ball-milling method. A weighed amount of LiH and LiNH$_2$, together with 20 steel balls (6 mm in diameter) and each additive, was put into a milling vessel made of steel of which the inner volume is about 70 cm^3, where the amount of LiNH$_2$ and LiH powders with 1:1 molar ratio and 5 mol% additive is 300 mg. And then, the ball milling was performed under 0.6 MPa hydrogen (>99.999%) atmosphere for 2 h at 450 rpm using a planetary ball milling apparatus (QM-3SP4). The ball-to-powder weight ratio is about 90:1. To minimize the temperature increment of the samples, the milling process was paused for 30 minutes for every hour of milling. All the samples were handled in an Ar-filled (>99.999%) glove box (Mikrouna, China) equipped with a circulative purification system, in which the typical H$_2$O/O$_2$ levels are below 0.1 ppm.

2.2 Structural characterizations

The structural characteristics of the produced composites were examined by X-ray diffraction (XRD) measurement (AXS D8 ADVANCE, Bruker, German). The samples were covered by a polyimide sheet to protect the samples from oxidation during measurements. The N–H stretching modes of the amides were characterized by Fourier Transform IR spectrometer (FTIR) (TENSOR 27, Bruker, Canada) in transmission mode. The test samples were prepared by cold pressing a mixture of power samples and potassium bromide (KBr) powder at a weight ratio of 1:20 to form a pellet. Each spectrum was created from 16 scans averaged with a scan resolution of 4 cm^{-1}.

2.3 Thermal desorption and isothermal dehydrogenation measurements

The thermal desorption behaviour, the composition of the evolved gas, and the thermogravimetry-differential scanning calorimetry were studied using a synchronous thermal analysis (DSC/DTA-TG; Netzsch STA 449 F3 Jupiter®) combined with a thermal desorption mass spectroscopy (TDMS; Netzsch QMS 403 D Aëolos®, Germany) with a heating rate of 10 °C/min under 30 ml/min Ar gas flow. The dehydrogenation kinetics was measured using a Hy-Energy PCT evo commercial volumetric hydrogen storage capacity apparatus (Sieverts apparatus), which facilitates the accurate volumetric determination of the amount of evolved hydrogen. Typically, about 0.15 g sample was loaded into a stainless steel autoclave and evacuated. Then, the sample was rapidly heated to desired temperatures. Dehydrogenation at 250 °C and 300 °C was performed under a vacuum.

Results and discussion

3.1 The dehydrogenation properties of the alkali metal hydroxide-doped LiNH$_2$−LiH system

In order to evaluate the effects of different alkali metal hydroxide, four composites of LiNH$_2$ and LiH without additive,

with LiOH additive, NaOH additive, and KOH additive were prepared by ball milling for 2 h at 450 rpm under hydrogen atmosphere of 0.6 MPa, and their dehydrogenation behaviours were determined by TDMS, as shown in Fig. 1. The method of ball milling is selected on the basis of our previous experiments to obtain a homogenous material.[26] It is notified that the scale of vertical axis in the TDMS profiles are all same, which make it convenient to compare the amount of hydrogen and ammonia released. For the composite without additive, two broad shaped hydrogen desorption curves and obvious ammonia emission are observed, which is in good agreement with the previous reports.[9–12] Interestingly, a significant enhancement of dehydrogenation properties is achieved by introducing KOH into the LiNH$_2$−LiH system, while the hydrogen desorption behaviours of the LiOH or NaOH-doped composites have no obvious change. In comparison with the broad shaped hydrogen desorption curve of the composite without additive, the hydrogen desorption curve of the LiNH$_2$−LiH−0.05 KOH composite becomes narrow. The dehydrogenation onset temperature of the composite with KOH additive is decreased by about 36 °C, and the dehydrogenation peak temperature is lowered by about 42 °C. Moreover, TDMS examination shows that almost no ammonia is released for the KOH-doped composite, indicating the evolution of ammonia is significantly suppressed due to the doping of KOH. However, there is still obvious ammonia emission in the hydrogen desorption process of the LiOH or NaOH-doped composites. It is therefore concluded that the effect of KOH on the dehydrogenation properties of the LiNH$_2$−LiH system is clearly better than those of the other two alkali metal hydroxides (LiOH and NaOH).
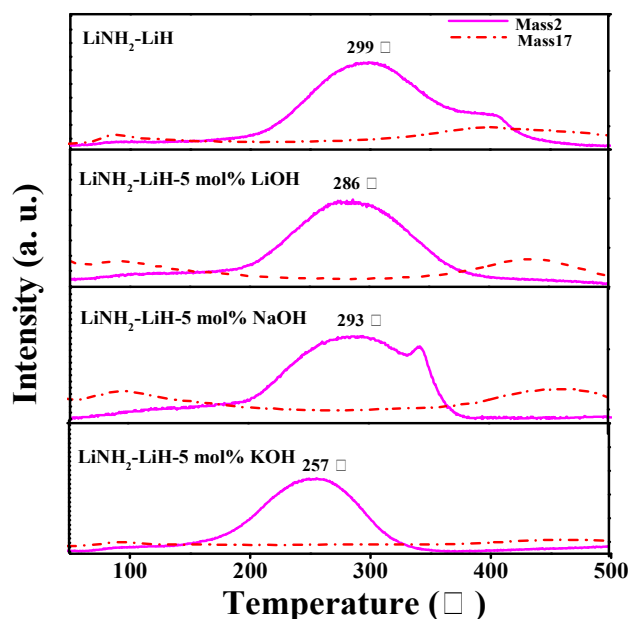
Fig. 1 The hydrogen and ammonia gas desorption mass spectra for each composite of LiNH$_2$ and LiH without additive, with 5 mol% LiOH additive, 5 mol% NaOH additive, or 5 mol% KOH additive.

3.2 The effects of KOH content on the hydrogen desorption properties of the LiNH$_2$−LiH system

To elucidate the effects of KOH content on the hydrogen desorption properties of the LiNH$_2$−LiH system, four composites of LiNH$_2$−LiH−x KOH with x=0.03, 0.05, 0.10, and 0.15 were prepared by ball milling for 2 h at 450 rpm under

hydrogen atmosphere of 0.6 MPa. As shown in Fig. 2, the compositional dependence of the dehydrogenation behaviours of the $LiNH_2-LiH-xKOH$ was examined by TDMS. Specifically, it can be seen that the hydrogen desorption peak temperature is gradually lowered with increasing KOH content from 3 mol% to 15 mol%. A 35 °C decrease for the dehydrogenation peak temperature is attained for the sample with 3 mol% KOH relative to the sample without additive as it is decreased from 299 °C to 264 °C. Further increasing the KOH content to 5 mol% induces an additional decline by 7 °C in the dehydrogenation peak temperature. More attractively, the side product of ammonia is distinctly retarded with doping 5 mol% KOH. The dramatically reduced ammonia impurity increases the purity of hydrogen released from the $LiNH_2-LiH$ system, which is very favourable for practical on-board applications as hydrogen storage material. It should be mentioned that, although further increasing the KOH content to 10 mol% or 15 mol% can result in an additional decline in the dehydrogenation peak temperature, the hydrogen capacity of this system will definitely be decreased with the amount of KOH increasing. The gas phases in the milling vessel after ball milling the 15 mol% KOH-doped $LiNH_2-LiH$ system was analyzed by GC (Fig. S1, in the supplementary information). There are no obvious ammonia signals in the GC profile, indicating that the obvious mass 17 signal of the 10-15 mol% KOH-doped $LiNH_2-LiH$ system in Fig 2 may due to other ion fragmentation, such as OH^-. Therefore, considering the hydrogen desorption and ammonia emission properties and hydrogen capacity, doping 5 mol% KOH will result in the best effect on the hydrogen desorption properties of the $LiNH_2-LiH$ system.
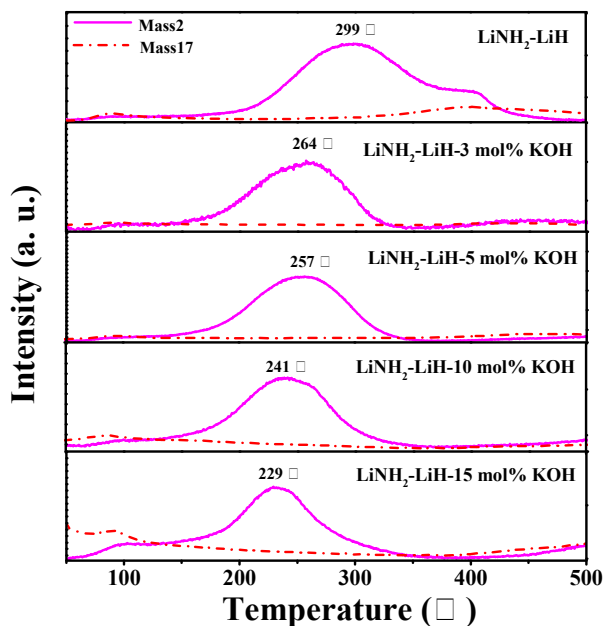
Fig. 2 The hydrogen and ammonia gas desorption mass spectra for each composite of $LiNH_2$ and LiH without additive, with 3 mol% KOH additive, 5 mol% KOH additive, 10 mol% KOH additive, or 15 mol% KOH additive.

The isothermal dehydrogenation behaviours of the $LiNH_2-LiH$ and $LiNH_2-LiH-0.05$ KOH samples at 250 °C and 300 °C are shown in Fig. 3. Apparently, doping 5 mol % KOH into the $LiNH_2-LiH$ system will result in a remarkable

improvement of desorption kinetics. At 250 °C, the $LiNH_2-LiH-0.05$ KOH sample releases about 2.9 wt% (30.0 mg/g) hydrogen within 0.6 h, but there is only about 1.9 wt% (19.1 mg/g) hydrogen released from the $LiNH_2-LiH$ sample. As the operating temperature is increased to 300 °C, about 3.8 wt% hydrogen is rapidly liberated from the $LiNH_2-LiH-0.05$ KOH sample within 0.4 h, while it will take over 1 h for the $LiNH_2-LiH$ sample to receive the same amount of hydrogen desorption. By analysing the slope of the linear parts, the maximum hydrogen release rate for the $LiNH_2-LiH-0.05$ KOH sample was estimated to be ~0.26 and 0.42 wt%/min at 250 °C and 300 °C, which are 1.6 and 1.3 times faster than that of the $LiNH_2-LiH$ samples (~0.16 and 0.33 wt%/min). Moreover, at temperatures of 250 °C and 300 °C the hydrogen desorption capacity for the $LiNH_2-LiH-0.05$ KOH sample is about 3.0 wt% and 3.9 wt% (Fig. 3), but the hydrogen desorption capacity for the $LiNH_2-LiH$ sample reaches about 3.2 wt% and 4.3 wt% (Fig. S2, in the supplementary information). The slightly decreased hydrogen desorption capacity for the $LiNH_2-LiH-0.05$ KOH sample is due to the addition of KOH with a larger molecular weight.
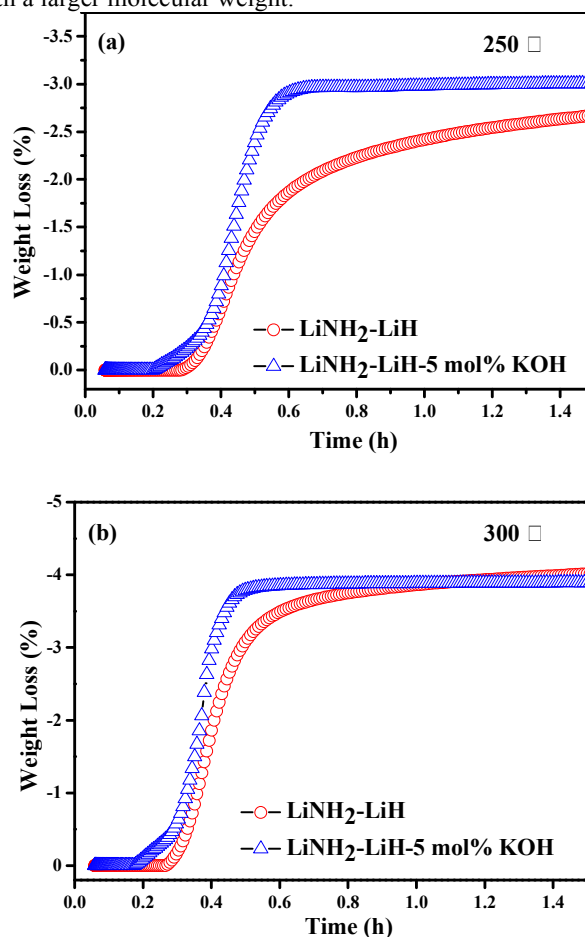
Fig. 3 Isothermal dehydrogenation curves of the $LiNH_2-LiH$ composites without additive or with 5 mol% KOH additive at 250 °C (a) and 300 °C (b).

3.3 The kinetic and thermodynamic analysis for the hydrogen desorption of the KOH-doped $LiNH_2-LiH$ sample

In general, the operating temperatures for hydrogen desorption of a hydrogen storage material are determined by two factors:

activation energy barrier and reaction enthalpy change. Here, the activation energy (E_a) was calculated with the Kissinger approach as follows.[27]

$$\frac{d\ln(\frac{\beta}{T_m^2})}{d(\frac{1}{T_m})} = -\frac{E_a}{R}$$

where T_m is the temperature at which the desorption rate is maximum, β is the heating rate, Ea is the activation energy and R is the gas constant. Fig. 4 shows the Kissinger plots of the $LiNH_2$–LiH and 5 mol% KOH-doped $LiNH_2$–LiH samples. By fitting the data points, an activation energy of 103.1 kJ/mol is obtained for the pristine $LiNH_2$–LiH sample, which is in good agreement with the previous results reported by L. F. Albanesi *et al.*[28] For the 5 mol% KOH-doped sample, the Ea value is calculated to be 58.2 kJ/mol. In comparison with the $LiNH_2$–LiH sample, a ~43 % reduction in the activation energy is obtained for the 5 mol% KOH-doped sample. These data suggest that additive of KOH is indeed effective for decreasing the activation energy of the $LiNH_2$–LiH system. It also indicates that the decline in the activation energy should be one of the important reasons for the decreased the dehydrogenation temperatures of the $LiNH_2$–LiH−5 mol% KOH sample.
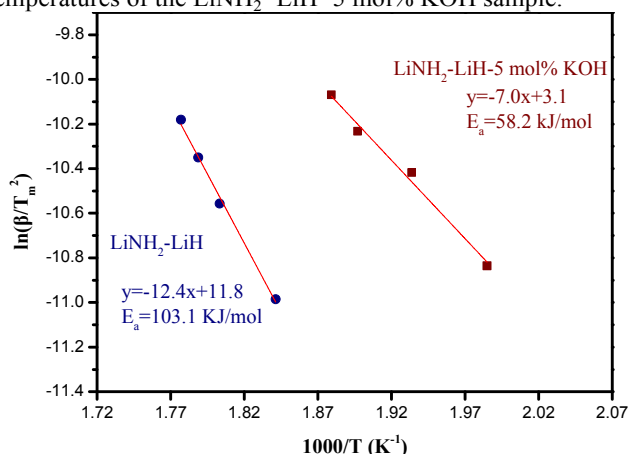
Fig. 4 Kissinger's plots of the $LiNH_2$–LiH and $LiNH_2$–LiH−5 mol% KOH samples.

As shown in Fig. 5, the heat effects of the composites with and without KOH additive in the process of desorption were determined by means of DSC. It is very interesting that the $LiNH_2$–LiH composite exhibits two endothermic peaks, a large one and a small one, whereas the KOH-doped $LiNH_2$–LiH composite shows a single endothermic peak. Integration of the endothermic peak delivers a heat effect of about 47.5 kJ/mol-H_2 for the $LiNH_2$–LiH composite, which is in agreement with the previous report.[6] For the $LiNH_2$–LiH−0.05 KOH composite, the overall heat effect is estimated to be about 45.1 kJ/mol-H_2, indicating that the overall enthalpy change for hydrogen desorption from the 5 mol% KOH-doped composite is slightly decreased, compared with that of the $LiNH_2$–LiH composite. Kinetic analysis shows that, in comparison with the $LiNH_2$–LiH sample, a ~43 % reduction in the activation energy is obtained for the 5 mol% KOH-doped sample. Therefore, we conclude that the decreased operating temperatures for hydrogen desorption of the $LiNH_2$–LiH−0.05 KOH sample mainly results from the corresponding reduction in the activation energy. In addition, Fig. 5 demonstrates that the endothermic onset and peak temperatures are gradually reduced

with the amount of KOH additive increasing, which further confirms the gradual reduction in the dehydrogenation temperatures of the KOH-doped composites as the amount of KOH increasing.
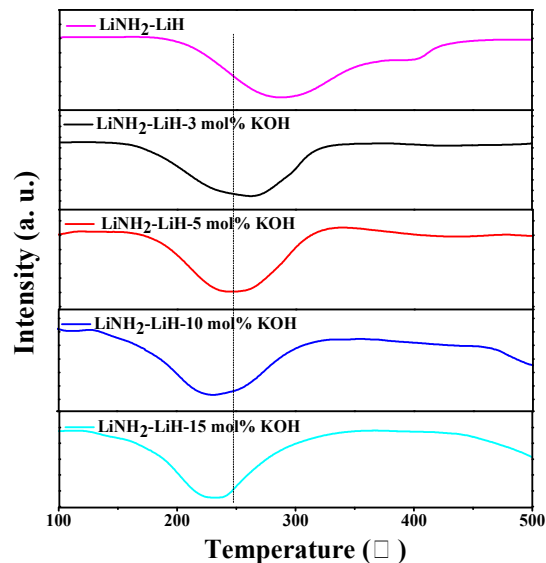
Fig. 5 The DSC profiles for each composite of $LiNH_2$ and LiH without additive, with 3 mol% KOH additive, 5 mol% KOH additive, 10 mol% KOH additive, or 15 mol% KOH additive.

3.4 The mechanism for the improvement of the hydrogen desorption properties in the KOH-doped $LiNH_2$–LiH sample

Fig. 6 shows the XRD patterns of the $LiNH_2$–LiH samples with and without alkali metal hydroxide after ball milling for 2 h. It is worth noting that, for the LiOH, NaOH, or KOH-doped samples after ball milling, the diffraction peaks due to the additive can not be observed, while the corresponding diffraction peaks due to alkali metal hydride and oxide phases can be observed in the XRD profiles. As reported previously, NaOH could react with LiH to produce NaH, Li_2O, and H_2,[29] which is consistent with our observation. In addition, potassium hydride and lithium oxide, of which the standard diffraction peaks are at 27.0°, 31.3°, 44.8°, 53.2° and 33.5°, 56.1°, 67.0°, respectively, is found for the KOH-doped $LiNH_2$–LiH sample after ball milling. This fact indicates that a solid reaction between the doped KOH and LiH takes place to convert to KH and Li_2O during ball milling (reaction 3).

$$KOH + 2LiH \xrightarrow{BM} KH + Li_2O + H_2 \uparrow \qquad (3).$$

The standard formation enthalpies of KOH, LiH, KH, and Li_2O are −424.6, −90.5, −57.7, and −597.9 kJ/mol, respectively.[30] As a result, the enthalpy change of the reaction (3) is calculated to be about −50.0 kJ/mol, exhibiting an exothermic nature. In other words, the solid reaction between KOH and LiH is thermodynamically favourable, which can be initialized by colliding balls during energetic ball milling.

Fig. 7 shows the FTIR spectra and XRD patterns of the $LiNH_2$–LiH samples with various amount of KOH after ball milling for 2 h. Only the typical doublet N−H vibrations of $LiNH_2$ at 3313/3259 cm^{-1} are observed in the FTIR spectrum, indicating that there are no reaction between the KOH and $LiNH_2$ converting to new amide or imide. It was found from the XRD profiles that the relative diffraction intensity of KH phase become stronger and stronger with the amount of KOH increasing, which indicates KH may play important roles in

improving the dehydrogenation kinetics in the KOH-doped $LiNH_2$–LiH systems, as the hydrogen desorption temperature is gradually lowered with increasing KOH content from 3 mol% to 15 mol% (Fig. 2).
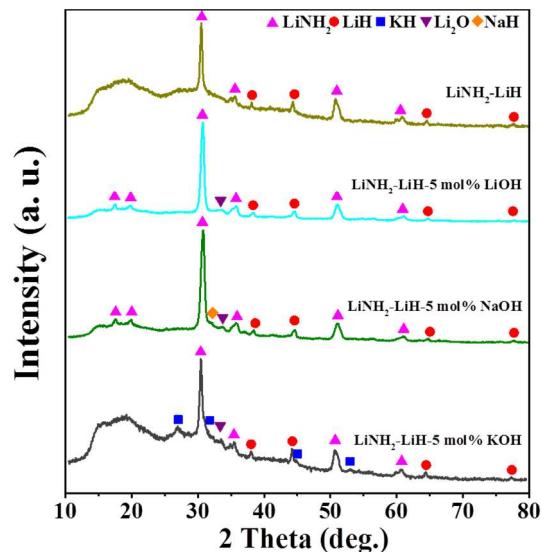
Fig. 6 The XRD profiles for each composite of $LiNH_2$ and LiH without additive, with 5 mol% LiOH additive, 5 mol% NaOH additive, or 5 mol% KOH additive after ball milling for 2 h.

Fig. 8 shows the FTIR spectra and XRD patterns for the dehydrogenated $LiNH_2$−LiH−0.05 KOH sample at different stages. The FTIR spectra and XRD patterns collected at 100 °C remain unchanged from the postmilled sample, since almost no hydrogen is released (Fig. 2 and Fig. 8). As the sample is heated up to 250 °C, no distinct change can be observed in the XRD pattern except that a small new diffraction peak at 33.1° due to $KLi_3(NH_2)_4$ is found. This phenomenon is consistent with the result that the ternary amide $KLi_3(NH_2)_4$ is inclined to be formed in the dehydrogenation/hydrogenation process of the potassium compounds-added Li–N–H system.[31,32] It is well known that the structural similarity makes it difficult to distinguish $LiNH_2$ and Li_2NH only by XRD. It can be observed from the FTIR spectra, after the dehydrogenation temperature is above 300 °C, a broad absorbance at around 3180 cm^{-1} due to the N−H stretching mode of Li_2NH is observed, in addition to the absorbance due to $LiNH_2$. Therefore, the diffraction peaks at 30.6°, 51.0° and 60.8° in the XRD profiles should originate from $LiNH_2$ and Li_2NH. With an gradual increase of the dehydrogenation temperature to 500 °C, the intensity of the N−H stretching modes due to $LiNH_2$ gradually decreased, but the intensity of the N−H stretching mode due to Li_2NH gradually increased. It is worth noting that, with increasing the temperature from 100 to 500 °C, the diffraction peaks of KH keep almost no changed, which also indicates KH acts as a catalyst in the whole dehydrogenation process declining the reaction energy barrier.

Recently, it was found that a few percentage (~5 mol%) of potassium hydride can significantly improve the hydrogen desorption kinetics of the LiH−NH_3 system.[25] In addition, remarkable enhancement in the kinetics of dehydrogenation is achieved by introducing 3 mol% KH into the $Mg(NH_2)_2$/2LiH system.[20] Such an improvement is further confirmed recently
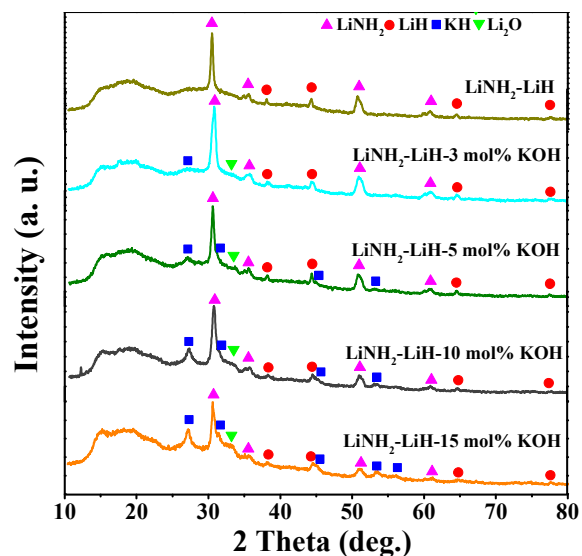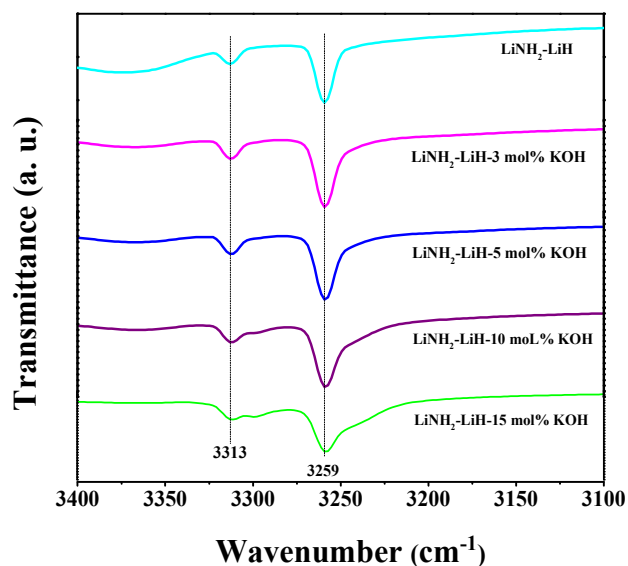
Fig. 7 The FTIR spectra and XRD profiles for each composite of $LiNH_2$ and LiH with 3 mol% KOH additive, 5 mol% KOH additive, 10 mol% KOH additive, or 15 mol% KOH additive after ball milling for 2 h.

by introducing KH into the $2LiNH_2$–MgH_2 system.[21] All these facts indicate that KH has good catalytic effect on improving the kinetic properties of dehydrogenation in the metal−N−H hydrogen storage systems. To further elucidate the reasons for the improvement of the hydrogen desorption properties in the potassium hydroxide-doped samples, the dehydrogenation behaviours of the $LiNH_2$−LiH−0.05 KH and $LiNH_2$−LiH−0.05 Li_2O was investigated by TDMS and compared with those of $LiNH_2$−LiH samples without additive and with KOH additive, as shown in Fig. 9. It was found that the $LiNH_2$−LiH−0.05 KH sample exhibits similar dehydrogenation behaviour to that of the $LiNH_2$−LiH−0.05 KOH sample. However, Li_2O has no catalytic effect on improving the dehydrogenation kinetics, as $LiNH_2$−LiH−0.05 Li_2O sample shows almost the same dehydrogenation behaviour with that of the $LiNH_2$−LiH

sample. Therefore, it is believed that the formation of KH is the primary reason for the improved dehydrogenation kinetics and the suppression of ammonia emission in the KOH-doped $LiNH_2-LiH$ system.
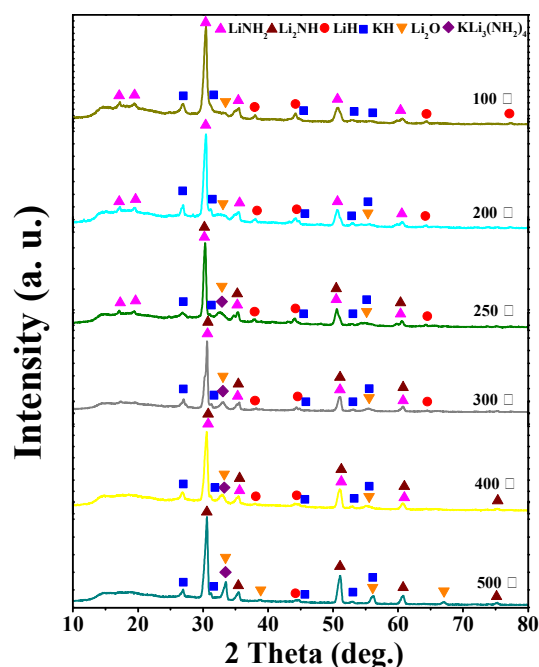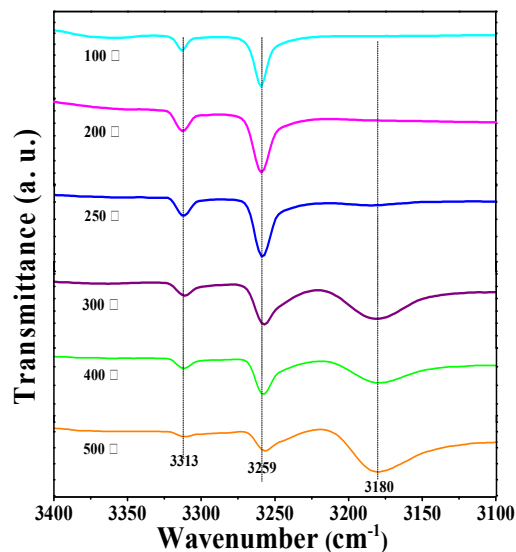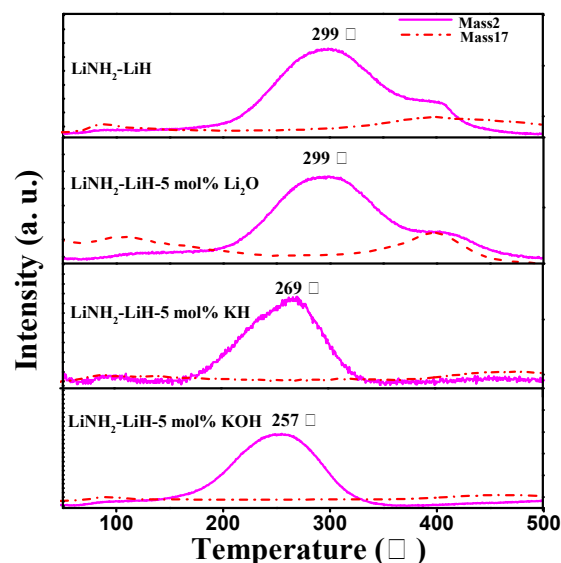
Fig. 9 Weight loss percent due to TG analysis and the hydrogen and ammonia gas desorption mass spectra for each composite of $LiNH_2$ and LiH without additive, with 5 mol% Li_2O additive, 5 mol% KH additive, or 5 mol% KOH additive.

Conclusions

In conclusion, the hydrogen desorption properties of the $LiNH_2-LiH$ system with alkali metal hydroxide (LiOH, NaOH, and KOH) were investigated and discussed. It was found that the three kinds of hydroxides are effective to enhance the hydrogen desorption properties of the $LiNH_2-LiH$ system, among which, KOH shows the best effect. In comparison with that of the $LiNH_2-LiH$ composite, the hydrogen desorption curve of the $LiNH_2-LiH-0.05$ KOH composite becomes narrow and the dehydrogenation onset and peak temperatures are decreased by about 36 °C and 42 °C, respectively. Isothermal desorption kinetics at 250 °C and 300 °C clearly reflect the dramatically improved kinetic properties. Kinetic and thermodynamic analysis shows that the improved operating temperatures for hydrogen desorption of the $LiNH_2-LiH-0.05$ KOH sample mainly results from the corresponding reduction in the activation energy. Detailed structural investigations reveal that during ball milling, the doped alkali metal hydroxide can react with LiH to convert to alkali metal hydride, which is responsible for the improvement in hydrogen desorption properties of $LiNH_2-LiH$ system.

Acknowledgements

Notes and references

College of Chemistry and Chemical Engineering, Yangzhou University, Yangzhou, 225002, P. R. China. E-mail: ylteng@yzu.edu.cn (Y.-L. Teng); Tel./fax: +86 514 87975590 9201.
Electronic supplementary information (ESI) available: GC profiles of gas phases in the milling vessel after ball milling the 15 mol% KOH-doped

Fig. 8 The FTIR spectra and XRD patterns for the dehydrogenated $LiNH_2-LiH-0.05$ KOH samples at different stages.

LiNH$_2$–LiH system under hydrogen atmosphere, Isothermal dehydrogenation curves of the LiNH$_2$–LiH composites at 250 °C and 300 °C. See DOI: 10.1039/b000000x/

1   C. W. Hamilton, R. T. Baker, A. Staubitz and I. Manners, *Chem. Soc. Rev.*, 2009, **38**, 279.

2   J. Yang, A. Sudik, C. Wolverton and D. J. Siegel, *Chem. Soc. Rev.*, 2008, **39**, 656.

3   P. Jena, *J. Phys. Chem. Lett.*, 2011, **2**, 206.

4   L. Schlapbach and A. Züttel, *Nature*, 2001, **414**, 353.

5   W. Grochala and P. P. Edwards, *Chem. Rev.*, 2004, **104**, 1283.

6   P. Chen, Z. T.Xiong, J. Z.Luo, J. Y. Lin and K. L. Tan, *Nature*, 2002, **420**, 302.

7   P. Chen, Z. T. Xiong, J. Z.Luo, J. Y. Lin and K. L. Tan., *J. Phys. Chem. B*, 2003, **107**, 10967.

8   S. I. Orimo, Y. Nkamori, J. R. Eliseo, A. Züttel and C. M. Jensen, *Chem. Rev.*, 2007, **107**, 4111.

9   Y. L. Teng, T. Ichikawa and Y. Kojima, *J. Phys. Chem. C.*, 2011, **115**, 589.

10 T. Ichikawa, N. Hanada, S. Isobe, H. Y. Leng and H. Fujii, *J. Alloys Compd.*, 2005, **404**, 435.

11 T. Zhang, S. Isobe, Y. Wang, N. Hashimoto and S. Ohnuki, *ChemCatChem*, 2014, **6**, 724.

12 S. Nayebossadri, K. F. Aguey-Zinsou and Z. X. Guo, *Int. J. Hydrogen Energy*, 2011, **36**, 7920.

13 R. A. Varin and M. Jang, *J. Alloys Compd.*, 2011, **509**, 7143.

14 W. I. F. David, M. O. Jones, D. H. Gregory, C. M. Jewell, S. R. Johnson, A.Wallton and P. P. Edwards, *J. Am. Chem. Soc.*, 2007, **129**, 1594.

15 H. Y. Leng, Z. Wu, W. Y. Duan, G. L. Xia and Z. L. Li, Int. J. Hydrogen Energy, 2012, **37**, 903.

16 J. Z. Yang, D. C. Li, H. Fu, G. B. Xin, J. Zheng and X. G. Li, *Phys. Chem. Chem. Phys.*, 2012, **14**, 2857.

17 S. Nayebossadri, *Int. J. Hydrogen Energy*, 2011, **36**, 8335.

18 Y. J. Liu, Y. Cheng, T. Ohba, K. Kaneko and H. Kanoh, *Int. J. Hydrogen Energy*, 2011, **36**, 12902.

19 T. F. Zhang, Y. Isobe, Y. M. Wang, H. Oka, N. Hashimoto and S. Ohnuki, *J. Mater. Chem. A*, 2014, **2**, 4361.

20 J. H. Wang, T. Liu, G. T. Wu, W. Li, Y. F. Liu C. M.Araújo, R. H. Scheicher, A. Blomqvist, R. Ahuja and Z. T. Xiong, *Angew.Chem. Int. Ed.*, 2009, **48**, 5828.

21 W. F. Luo, V. Stavila and L. E. Klebanoff, *Int. J. Hydrogen Energy*, 2012, **37**, 6646.

22 J. H. Wang, G. T. Wu, Y. S. Chua, J. P. Guo, Z. T. Xiong, Y. Zhang, H. G. Pan and P. Chen, *Chem. Sus. Chem.*, 2011, **4**, 1622.

23 C. Liang, Y. F. Liu, M. X. Gao and H. G. Pan, *J. Mater. Chem. A*, 2013, **1**, 5031.

24 Y. F. Liu, C. Li, B. Li, M. X. Gao and H. G. Pan, *J. Phys. Chem. C*, 2013, **117**, 866.

25 Y. L. Teng, T. Ichikawa, H. Miyaoka and Y. Kojima, *Chem. Commun.*, 2011, **47**, 12227.

26 B. X. Dong, L. Song, Y. L. Teng, J. Ge and S. Y. Zhang, *Int. J. Hydrogen Energy*, 2014, **39**, 13838.

27 H. E. Kissinger, Anal. Chem., 1957, **29**, 1702.

28 L. F. Albanesi, P. A. Larochette and F. C. Gennari, *Int. J. Hydrogen Energy*, 2013, **38**, 12325.

29 M. Kawakami, T. Kuriiwa, A. Kamegawa, H. Takamura, M. Okada and T. Kaburagi, *Mater. Trans.*, 2009, **50**, 1855.

30 W. M. Haynes, CRC handbook of chemistry and physics, 93rded.; CRC press/taylor and Francis: Boca Raton, FL, 2012.

31 B. X. Dong, L. Song, J. Ge, Y. L. Teng and S. Y. Zhang, *RSC Adv.*, 2014, **4**, 10702.

32 B. X. Dong, Y. L. Teng, J. Ge, L. Song and S. Y. Zhang, *RSC Adv.*, 2013, **3**, 16977.